Modelling percolation in fibre and sphere mixtures: routes to more efficient network formation

Sameer S Rahatekar[1†], Milo S P Shaffer[2] and James A Elliott[1*]

1. Department of Materials Science and Metallurgy, University of Cambridge, Pembroke Street, Cambridge CB2 3QZ, UK.

2. Department of Chemistry, Imperial College London, SW7 2AZ, UK.

†Present address: Advanced Composites Centre for Science & Innovation (ACCIS), University of Bristol, 83 Woodland Road, Bristol, BS8 1US, UK.

* Corresponding author: jae1001@cam.ac.uk

Mixtures of perfectly conducting fibres and spheres, as well as mixtures of fibres of different aspect ratios, were simulated using a Dissipative Particle Dynamics (DPD) method, and the connectivity of the resulting assemblies was analyzed using a Monte Carlo algorithm to predict the threshold volume fraction of filler material required for electrical percolation. For both isotropic and uniaxially oriented fibre-sphere mixtures, it was found that gradually replacing fibres with an equivalent volume of spheres increased the percolation threshold. By contrast, in aligned mixtures of fibres of two different aspect ratios, replacing a small fraction of higher aspect ratio fibres with shorter fibres lead to a reduction in the percolation threshold, since the shorter fibres orient less well and provide bridging links between the highly oriented longer fibres. These theoretical results suggest that mixtures of fibres of different aspect ratio may be helpful in reducing the volume fraction of high aspect ratio filler particles (such as multi-wall carbon nanotubes) required to achieve significant electrical conductivity in composite materials.

Keywords: A. Nano composites, A. Polymer-matrix composites (PMCs), B. Electrical properties, C. Modelling, fibre-sphere mixtures

1. Introduction

The formation of extended networks of particles dispersed in a fluid gives rise to a discontinuous change in the rheological [1-5] and electrical [6-9] properties of the dispersion at concentrations around the so-called percolation threshold. Historically, percolation theory was first used by Flory [10] to explain the phenomenon of gelation in thermosetting polymers. Scher and Zallen [11] used percolation theory to study the insulator-to-conductor transition in disordered mixtures of conducting and non-conducing spheres, establishing a threshold around 15 vol%. Pike *et al.* [12] and Balberg *et al.* [13-14] extended the application of percolation theory to study network formation using randomly-orientated anisotropic particles, as a function of volume fraction, and electrical percolation in carbon nanotube polymer composites was recently reviewed by Bauhofer and Kovacs [15]. Several researchers have attempted to predict the effect of fibre aspect ratio and orientation distribution on the critical volume fraction required to achieve a percolating network [16-20]. However, all of these approaches tend to ignore the fibre-fibre and fibre-dispersion medium interactions other than the effects of excluded volume. It has been shown experimentally that additional forces, such as those mediated by shear or external electric field interactions, play an important role in the formation of fibre networks, and hence the onset of percolation [21, 22]. In a previous work by some of the present authors [23], a novel method was described in which dispersions of nanofibres were studied by carrying out Dissipative Particle Dynamics (DPD) simulations for systems with different aspect ratios and degrees of fibre alignment. For each configuration so generated, Monte Carlo simulations were then performed in order to determine the critical volume fraction of fibres required to achieve electrical conductivity. It was shown that randomly oriented, high aspect ratio fibres are effective in achieving percolation at low volume fractions, but lose their advantage when highly aligned; whereas low aspect ratio fibres, on the other hand, are relatively insensitive to fibre alignment. In the present study, we investigate the possibility of reducing the percolation threshold of aligned fibres by mixing fibres of two aspect ratios, starting with the limiting case of a mixture of spheres (i.e. aspect ratio of unity) and fibres of varying degrees of alignment. The results are relevant to understanding rheological [24] and phase behaviour [25-29], as well as computer simulation studies [30-33] of rod-sphere mixtures. The experimental relevance of such work is demonstrated in a recent paper by Sumfleth *et al.* [34], who found that for an conductive epoxy nanocomposite, a considerable amount of multi-wall carbon nanotubes (MWCNTs) can be

replaced by carbon black (CB) without changing the electrical properties. Since MWCNTs are currently more expensive than CB per unit mass, this may have important cost implications for the manufacture of electrically conductive composites. In general, the current study of mixtures of fibres and spheres and mixtures of fibres of different aspect ratios will also be an important first step in understanding the effect of particle shape polydispersity on the onset of percolation. The remainder of the paper is structured as follows. In Section 2, we briefly summarise the methods for generating and analysing the fibre networks. We then describe results from the consideration of an isotropically oriented ensemble of fibres with a single aspect ratio (Section 3.1). Next, the fibres are replaced stepwise by spheres of equivalent volume, and the effect on the percolation threshold as a function of total particle volume is studied (Section 3.2). The relative contribution of the fibres and spheres in the formation of percolating the network are studied using a Monte Carlo simulation method (Section 3.3). Finally, in Section 3.4, the percolation threshold in binary mixtures of fibres with different aspect ratios is also studied using a similar methodology.

2. Modelling Methodology

In 1992, Hoogerbrugge and Koelman [35] introduced a method called Dissipative Particle Dynamics (DPD), which is similar to molecular dynamics, but applied on a supramolecular scale. The dynamics of a system of particles is coarse-grained by calculating the motion of particle clusters subjected to pair-wise, dissipative and random forces. Español and Warren [36] improved on the DPD model originally proposed by Hoogerbrugge and Koelman. In this work, they showed that the temperature of the system was directly related to the amplitude of the noise by means of a fluctuation dissipation theorem. Since then, DPD has been used to model wide variety of problems including, for example, shear thinning behaviour of polymer solutions [37], prediction of phase separation [38], and the suspension phenomenology of particles with different shapes [39-41].

In the current work, we represent the fibre as collection of fused spheres, as shown in Fig 1a. Conservative (F^C), dissipative (F^D) and random (F^R) forces, given by equations (1)-(3), are defined between each pair of spheres that are not part of the same fibre. Although the conservative interaction (F^C) is only softly repulsive, an effective hard-sphere diameter can be assigned based on a correspondence described in our previous paper [23]. Together with the

number of spheres comprising each fibre, this can be used to define the fibre volume, taking into account any overlap of the spheres in each fibre, and hence the volume fraction of fibres in the periodic cell volume.

$$\mathbf{F}_{i,j}^{\mathrm{C}} = \left(\frac{n\varepsilon_{i,j}}{\sigma_{i,j}} \right) \omega^{\mathrm{C}} \left(\frac{\sigma_{i,j}}{r_{i,j}} \right)^{n+1} \hat{\mathbf{r}}_{i,j} \qquad (1)$$

$$\mathbf{F}_{i,j}^{D} = -\kappa \omega^{D} \mathbf{r}_{i,j} \cdot \mathbf{v}_{i,j} \hat{\mathbf{r}}_{i,j} \qquad (2)$$

$$\mathbf{F}_{i,j}^{\mathrm{R}} = \eta \, \omega^{\mathrm{R}} \theta_{i,j} \Delta t^{-1/2} \hat{\mathbf{r}}_{i,j} \qquad (3)$$

The forces act between pairs of spheres *i* and *j* whose centres are connected by a vector $\mathbf{r}_{i,j}$ and travel with relative velocity $\mathbf{v}_{i,j}$. The parameters $\varepsilon_{i,j}$ and $\sigma_{i,j}$ define the relative sizes of the spheres, and $\theta_{i,j}$ are a set of Gaussian random numbers with zero mean and unit variance. The repulsive exponent *n* was set to 12 to limit the interpenetration of the fibres [23]. The friction coefficient, κ, and the noise amplitude, β, are connected by equation (4) [36].

$$\eta^2 = 2 \kappa k_{\mathrm{B}} T_{\mathrm{eq}} \qquad (4)$$

The random force together with the dissipative force produces an effect as if the fibres are suspended in the pseudo-fluid. In principle, one can take into account the effect of alignment of the fibres due to an external field, such as shear or electric field. We start by carrying out DPD simulations of rigid fibre assemblies, where the initially aligned array of fibres relaxes to an isotropic orientation when no external forces are applied on the fibres. The orientation of the fibres is measured by a nematic order parameter *s* defined by equation (5) [42].

$$s = \frac{1}{2}\left[3\left\langle \cos^2 \theta \right\rangle - 1\right] \qquad (5)$$

Once the fibres are relaxed to isotropic orientation, ($s = 0$), a Monte Carlo walk of a virtual "electron" through the now fixed ensemble of fibres is carried out, driven by the presence of a uniform external electric field. It is assumed that the electron can move freely along each fibre; however, the probability for it to move to an adjacent fibre is given by equation (6) [23].

$$p_t = \exp\left(-\frac{D}{\gamma}\right)\exp\left(-\frac{\varepsilon\Delta x}{k_B T}\right) \quad (6)$$

where D is the closest distance between fibres, ε is the product of the applied electric field strength and charge on the "electron", k_B is the Boltzmann's constant, T is temperature in Kelvin, γ is related to the dielectric tunnelling length and Δx is the length of D along the direction of the external electric field. The first part of equation (6), $\exp(-D/\gamma)$, is related to the probability of quantum tunnelling of the "electron" between the fibres. The tunnelling probability decreases exponentially with increasing distance between the fibres, and is restricted to be less than unity since D and γ are always positive. The second part of equation (6), $\exp(-\varepsilon\Delta x/k_B T)$, will tend to drive the "electron" to move preferentially in the direction of the external electric field. Again, it cannot exceed unity since all terms in the expression are positive. The product, p_t, must therefore lie between zero and unity.

During each Monte Carlo step, the "electron" is displaced randomly to an adjacent fibre, with the acceptance probability of such a move given by equation (6). If the fibres form a percolating network, the virtual "electron" will travel a large distance during its Monte Carlo walk; if not, the "electron" will tend to become trapped in the local pocket of fibres. The distance travelled by the "electron" in a fixed time, averaged over many MC runs, gives the average flux of particles per unit area. In this way, it is possible to use the distance travelled by the electron during fixed number of Monte Carlo walk to find the critical percolation threshold. In our previous study, we predicted the percolation threshold for monodisperse fibres as a function of fibre aspect ratio and fibre orientation [23].

3. Results

3.1 Predicting the percolation threshold in fibre-sphere mixtures

The simplest case of a binary mixture fibre-sphere was examined using a mixture of fibres with aspect ratio $\lambda = l/d = 20$ and spheres of diameter d. Both the fibres and spheres interact with each other by soft-core repulsive forces along with the dissipative and random forces, as described by equations (1) to (3). The initial configuration consisted of uniaxially aligned array of pure fibres which was allowed to relax to find the percolation threshold for randomly oriented fibres. Then, step-by-step, the fibres were replaced with the number of spheres required to maintain a constant

total volume fraction. As an example, Fig. 1a shows an equilibrium mixture of fibres and spheres with total particle volume fraction of 0.085, and a volume fraction of spheres relative to the total particle volume (Φ_{rs}) of 10% (note that the number fraction is considerably larger). Fig. 1b shows an equilibrium mixture with total volume fraction 0.095 and $\Phi_{rs} = 0.5$. In these examples, the fibres have relaxed to a random orientation ($s = 0$), and the spheres are randomly dispersed without any spatial correlation (as confirmed by the radial distribution function (RDF) plot). Having established equilibrium particle arrangements using DPD, the Monte Carlo method (using two MC million steps) was used to probe the existence of percolating networks in the binary mixture. Fig. 2 shows the normalised distance travelled (*i.e.* total distance travelled divided by the number of MC steps) as a function of the total volume fraction of the particles. Such a plot can be used to find the percolation transition for sphere-fibre mixtures with different relative volume fractions of spheres by fitting a power-law expression in the vicinity of the percolation transition [23]. Fig. 3 shows the critical volume fraction required for percolation as a function of the relative volume fraction of spheres (Φ_{rs}) in the fibre sphere mixture. As can be seen, when the fibres are replaced with spheres of equivalent volume in the sphere-fibre mixture, the critical total volume fraction required to achieve percolation rises. The effect is expected, since randomly oriented fibres form networks more efficiently than spheres. During the set of simulations required to calculate each data point, the relative volume fraction of fibres to spheres was kept constant while the total volume fraction of the particles was varied in order to find the percolation threshold.

For the two pure systems, the values tended to the expected [23] percolation thresholds of 0.028 for fibres ($\lambda = 20$) and 0.15 for spheres. For intermediate compositions, the percolation threshold increased monotonically with increasing relative volume fraction of spheres in the mixture. As the fibres were initially replaced by spheres, the fibres continue to dominate the percolating network formation. The black line in Fig. 3 is given by $\Phi_{crit} + \Phi_{crit}\left\{\Phi_{rs}/\left(1-\Phi_{rs}\right)\right\}$; in other words, the expected total volume fraction at the percolation threshold if the sphere fraction makes no active contribution to the network. This simple projection of the fibre-only contribution fits well over relatively low relative volume fractions of spheres, showing that, in this range, the contribution made by spheres towards percolation is insignificant. However, on raising the relative volume fractions of spheres (above around $\Phi_{rs} = 0.7$ for $\lambda = 20$), there is a clear deviation from the fibre-only projection, showing that the spheres begin to contribute

significantly. Once the spheres have a controlling influence, the percolation threshold rises rapidly as the network increasingly consists of relatively inefficient particles. To understand this behaviour further, the Monte Carlo data were studied more closely in order to establish which particles were visited most frequently by the virtual "electron".

3.2 Frequency of visits during Monte Carlo Walk to Study the Network Properties

Goulet *et al.* [43] analysed visit frequencies during Monte Carlo "electron" walks in order to identify the critical connections in pure fibre networks. For the current study, the same algorithm was applied to fibre-sphere mixtures; the visit to a given particle is counted only when the "electron" moves onto that site from a different particle, and not for those steps in which it stays resident on the same particle. Each Monte Carlo walk (10^6 steps) was repeated ten thousand times, from random starting points, in order to obtain good counting statistics (no difference was observed between data collected over 5000 and 10000 repeats). Each fibre or sphere was then categorised (and coloured for visualisation) according to the number of visits; an example is shown in Fig. 4a. The light green colour represents the least visited fibre or sphere, and the red colour represents most frequently visited fibre or sphere. From the colour distribution, it is clear that the fibres are much more frequently visited than the spheres in this example based on a low relative fraction ($\Phi_{rs} = 0.05$) of spheres. This visual impression is confirmed by the histogram of visit frequencies shown in Fig 4b; the distributions are quite different, with the majority of the fibres playing a significant role in the network, and the majority of the spheres showing the minimum number of visits. An example of the sphere-dominated mixtures ($\Phi_{rs} = 0.9$) is shown in Fig. 5; in this case, most of the spheres are visited during at least ten percent of the Monte Carlo passes and some of the spheres are visited more often. In the $\Phi rs = 0.05$ example, most of the spheres were not visited at all. This analysis therefore indicates that at low relative volume fractions of the spheres, the percolation is achieved mainly via the network of the fibres. However, when the relative volume fraction of the spheres is high, the fibres alone do not form a percolating network alone and the spheres begin to participate. The data are thus consistent with the transition proposed above between a fibre and a sphere-dominated network.

3.3 Percolation in the binary mixture of fibres of different aspect ratios

Having studied fibre-sphere case, we next investigated percolation in binary mixtures of fibres with different aspect ratios. For the purpose of the current simulations, a mixture of fibres of λ = 20 and λ = 5 were chosen. This combination ensures a sufficient distinction between the fibres, whilst maintaining a reasonable overall size for the simulation. Both types of fibres interact with each other via soft-core repulsive forces along with the dissipative and random forces as before. Initially, monodispersed fibres with λ = 20 were simulated using DPD; subsequently, ten volume percent of the λ = 20 fibres were replaced with an equivalent volume of λ = 5 fibres. The goal of these simulations was to study the relationship between percolation threshold and the relative orientation of the fibres in the binary mixture.

The simplest case involves a random orientation of both types of fibres. After the DPD simulation is commenced, the λ = 20 fibres achieve an isotropic orientation ($s_{\lambda 20}$ = 0), as measured by order parameter defined in equation (5), more slowly than the λ = 5 fibres in the binary mixture. Also, the level of fluctuations in the average order parameter for the ensemble of λ = 5 fibres is larger than that for the λ = 20 fibres. This difference can be attributed to both the smaller absolute number of λ = 5 fibres and their lower moment of inertia. The order parameter of both λ = 20 and λ = 5 fibres, and hence the total order parameter of the binary mixture, reaches zero (*i.e.* isotropic orientation) since there are no external forces applied on the fibres, and the total volume fraction is well below the isotropic-nematic transition point [32]. After an equilibrated configuration of the binary fibre mixture was achieved, the conductivity was assessed using the Monte Carlo analysis, as shown in Fig. 6. As might be expected qualitatively, the critical percolation volume fraction for randomly oriented fibres of λ = 20 increased from 0.028 for monodispersed fibres to 0.033 after partial substitution with shorter fibres. In other words, for isotropically oriented fibres, higher aspect ratio fibres are most effective in achieving a percolating network at low volume fractions.

Previously, we showed [23] that when high aspect ratio fibres become aligned in the direction of an external field (such as shear or electric field), the percolation threshold required to achieve conductivity rises dramatically. It was also shown that low aspect ratio fibres are less sensitive to changes in percolation threshold due to alignment. In order to study the effect of orientation on the mixed fibre system, the λ = 20 fibres were aligned (to order parameter $s_{\lambda 20}$ = 0.9) using the

external electric field method reported previously [23]. Briefly, it is well known [22, 44, 45] that conducting fibres become polarised in presence of external electric field and experience a torque that tends to align them in the direction of the field. In our model, polarisation of the fibres is modelled by the introducing a fixed permanent dipole moment that interacts only with the external electric field. The degree of alignment of the fibres can then be controlled by changing the strength of the external electric field and the magnitude of charges in the dipole [23]; dipole-dipole interactions between fibres are ignored. In effect, the external electric field serves only as a means of producing the desired state of orientation of the fibres, and its magnitude (together with that of the imposed dipole moment) is arbitrary.

Once again, 10 vol% of the primary fibres were replaced by shorter ($\lambda = 5$) fibres; however, no dipole was added to the shorter fibres which, therefore, maintained a random orientation. In a more realistic situation, the shorter fibres might be oriented but to a lesser extent than the long fibres (since they experience less torque and more rapid thermal disordering). However, randomly oriented shorter fibres represent an interesting and simple limiting case. Having calculated the individual order parameters of $\lambda = 20$ and $\lambda = 5$ fibres in the binary mixture, we confirmed that the shorter fibres were less oriented than the longer fibres, with an overall average order parameter of $s_{mixture} = 0.58$. Fig. 7a compares the percolation transition for this binary mixture with randomly oriented monodispersed fibres of $\lambda = 20$ and $\lambda = 5$ ($s_{\lambda 20} = 0$ and $s_{\lambda 5} = 0$). The mixture of fibres achieves percolation at lower volume fraction than that for monodispersed $\lambda = 5$ fibres. However the mixture of fibres shows a higher percolation threshold than that for the randomly oriented monodispersd fibres of $\lambda = 20$. Fig. 7b compares the percolation threshold in the mixture of fibres with the percolation threshold of aligned monodispersed fibres of $\lambda = 20$ ($s_{\lambda 20} = 0.9$). The mixture of fibres can achieve a lower percolation threshold than that for aligned monodispersed fibres of $\lambda = 20$ ($s_{\lambda 20} = 0.9$). Hence, by replacing a small fraction of aligned $\lambda = 20$ fibres with randomly oriented $\lambda = 5$ fibres, it is possible to significantly decrease the percolation threshold.

Although it might be possible to arrange short fibres randomly oriented around longer fibres, such a situation is unlikely from a practical point of view. More plausibly, both long and short fibres would experience an aligning force, due for example to an applied shear, electric, or magnetic field, resulting in two different orientation distributions. To this end, dipoles were

introduced to both sets of fibres ($\lambda = 5, 20$, $\Phi_r = 0.1$, as before) to interact with the external electric field, so that they become aligned; the same virtual charge was applied at the ends of each fibre. As was confirmed from the calculated order parameters, both $\lambda = 20$ and $\lambda = 5$ fibres become aligned in the direction of external field. The order parameter for $\lambda = 20$ fibres fluctuated around $< S_{\lambda 20} > = 0.9$, whereas the order parameter for the $\lambda = 5$ fibres fluctuated around $< S_{\lambda 5} > = 0.57$, with the net order parameter of the binary mixture around $< S_{mixture} > = 0.78$. The difference in order parameter between the short and long fibres can be attributed partly to the greater dipole separation for high aspect ratio fibres, which results in a higher torque due to the external electric field. Hence, the degree of alignment for the longer fibres is higher than that for the shorter fibres even if strength of the applied electric field is the same for both. More specifically, Fishbine [46] have used following expression for dipole moment acting on the polarised rod :

$$p_x = \varepsilon_o E_x \frac{V}{L} \hat{x} \tag{7}$$

where ε_o is the free space permittivity, E_x the applied field component along the *x*-direction, *V* is the volume of the object and *L* is the depolarization coefficient. The depolarization coefficient for elongated objects was given by Behroozi *et al.* [44] as:

$$L = \left(6 \frac{a^2}{d^2} \right) \left\{ \ln \left[\frac{2d}{a} - \frac{7}{3} \right] \right\} \tag{8}$$

where *d* is the length and *a* is the radius of the elongated object. From Eq. 8, it can be deduced that the depolarization coefficient for $\lambda = 5$ fibres is more than one order of magnitude higher than that for $\lambda = 20$ fibres. So, in a fixed external field, the longer fibres will experience higher dipole moment than shorter fibres, and hence may be expected to show higher alignment, which is qualitatively consistent with our simulation results, although the real difference in orientation due to a change in aspect ratio is likely to be even greater. Previous work modelling fibres under shear [47] and analysing conducting rods in electric fields [48] reports similar trends. Clearly, the exact nature of the relative orientation distributions in a real situation will depend on the experimental conditions (temperature, field type, field strength, polarisability, moment of inertia, etc) but, in general, shorter fibers will be less strongly oriented.

As seen from Fig. 8a, the percolation transition for current binary mixture case study (Φ_{crit} = 0.052) was higher than that for the monodisperse fibres of λ = 20 at $S_{\lambda 20}$ = 0.0 (Φ_{crit} = 0.062). However for the percolation threshold of the mixture of fibres is lower than that for aligned monodispersed fibres of λ= 20 (Fig. 8b). The presence of short aspect ratio fibres (which are not as highly aligned as the high aspect ratio fibres) reduces the net order parameter of the binary mixture. But more significantly, the partially aligned short fibres act as a bridge between the highly aligned aspect ratio 20 fibres, maintaining the efficiency of the network. The effect is similar to the introduction of randomised short fibres to the aligned long fibres, but less strong, as the alignment of the short fibres reduces their network forming ability.

Conclusions

If percolation is required at low volume fractions in a system of fibres with high aspect ratio, the best strategy is usually considered to be the use of the highest aspect ratio particles feasible using the desired processing methods. The current theoretical study shows that this argument holds for randomly oriented systems; however, for any system that experiences a degree of alignment, for example due to magnetic, electric, or shear fields, then the addition of a small fraction of significantly shorter fibres is likely to beneficial. The long fibres dominate the transport but can become isolated once aligned; shorter fibres that orient less strongly can bridge between the long fibres. Clearly, the parameter space is large, given the range of absolute and relative concentrations, fibre dimensions, and orientations, but beneficial combinations exist and are worthy of further study. This model provides a means of exploring the behaviour of heterogeneous mixtures of particles and can readily be extended to other, non-fibrous shapes [38] as well as more complex and realistic polydispersed distributions of particles.

Acknowledgements

The authors gratefully acknowledge funding from US Army European Research Office under contract number N6255-020C9014. We wish to thank Klint A Rose and Prof Juan G Santiago for useful comments and discussions.

References:

[1] S B Kharchenko, J F Douglas, J Obrzut, E A Grulke, K B Migler, Nature Materials, **3** (8), 564 (2004).

[2] F. M. Du, R.C. Scogna, W. Zhou, S. Brand, J.E. Fischer, K. I. Winey, Macromolecules, **37** (24), 9048, (2004).

[3] S. S. Rahatekar, K.K.K. Koziol, S.A. Butler, J. A. Elliott, M. S. P. Shaffer, M.R. Mackley and A.H. Windle, Journal of Rheology, **50** (5), 599 (2006).

[4] E.K. Hobbie, D.J. Fry, Physical Review Letters, **97**(3), 036101, (2006).

[5] S. S. Rahatekar, K. K. Koziol, S. R. Kline, E. K. Hobbie, J. W. Gilman, and A. H. Windle, Advanced Materials, **21**, 874 (2009).

[6] J.N. Coleman, S. Curran, A.B. Dalton, A.P. Davey, B. McCarthy, W. Blau and R.C. Barklie, Physical Review B, **58**, 12 7492 (1998).

[7] B. E Kilbride, J. N. Coleman, J. Fraysse, P. Fournet, M. Cadek, A. Drury, S. Hutzler, S. Roth and W. J. Blau, Journal of Applied Physics, **92**, 4024, (2002).

[8] B. Vigolo, C. Coulon, M. Maugey, C. Zakri, P. Poulin, Science **309**, 920 (2005).

[9] E. J. Garboczi, K. A. Snyder, and J. F. Douglas, Physical Review E, **52**, 819 (1995).

[10] P. J. Flory, Journal of American Chemical Society, **63**, 3083, (1941).

[11] Zallen R, "The Physics of Amorphous Solids", John Wiley & Sons, 1983.

[12] G. E. Pike and C. H. Seager, Physical Review B, **10**, 1421 (1974).

[13] I. Balberg and N. Binenbaum, Physical Review B **28**, 3799, (1983).

[14] I. Balberg, N. Binenbaum, and N. Wagner , Physical Review Letters, **52**, 1465, (1984).

[15] W. Bauhofer and J.Z. Kovacs, Composites Science and Technology, **69**(10), 1486 (2009).

[16] S.H. Munson-McGee., Physical Review B, **43,** 3331, (1991).

[17] A.Celzard, E. McRae, C. Deleuze, M. Dufort, G. Furdin and J.F. Marêché, Physical Review B, **53**, 6209, (1996).

[18] T. Natsuki, M. Endo and T. Takahashi, Physica A **352**: 498, (2005).

[19] L Flandin, M. Verdier , B. Boutherin, Y. Brechet, J.Y. Cavaille, Journal of Polymer Science Part B-Polymer Physics **37**, 805, (1999).

[20] Foygel M, Morris RD, Anez D, French S, Sobolev VL, Physical Review B **71**: 104201, (2005).

[21] C.A Martin., J.K.W. Sandler, M.S.P. Shaffer, M.-K Swwarz, W. Bauhofer, K. Schulte, A.H. Windle, Composites Science and Technology, **64**, 2309, (2004).

[22] C. A. Martin, J. K. W Sandler, A. H. Windle, M.K. Schwarz, W. Bauhofer, K. Schulte and M. S. P. Shaffer, Polymer, **46**, 877 (2005).

[23] S. S. Rahatekar, M. Hamm, M. S. P. Shaffer, J. A. Elliott, Journal of Chemical Physics, **123**, 134702 (2005).

[24] I. Marti, O. Hofler, P. Fischer, E.J. Windhab, Rheologica acta, **44** , 502, (2005).

[25] Z. Dogic, D. Frenkel, S. Fraden, Physical Review E, **62**, 3925, (2000).

[26] M. Adams, Z. Dogic, S.L. Keller, S. Fraden, Nature **393**, 349, (1998).

[27] K. Lin, J.C. Crocker., A.C. Zeri, A.G. Yodh, Physical Review Letters, **87**, 088301, (2001).

[28] G.A. Vilegenthart, A. Van Blaaderen, H.N.W. Lekkerkerker, *Faraday Discussions* **112**, 173, (1999).

[29] M. Adams and S. Fraden, Biophysical Journal **74**, 669, (1998).

[30] D. Antypov, D.J. Cleaver , Chemical Physics Letters **377**, 311, (2003).

[31] D. Antypov, D.J. Cleaver, Journal of Chemical Physics **120**, 10307, (2004).

[32] P. Bolhuis, Journal of Chemical Physics **101**, 9869, (1994).

[33] T. Schilling, S. Jungblut, and M. A. Miller, Physical Review Letters **98**, 108303 (2007).

[34] J. Sumfleth, X. C. Androher and K. Schulte, Journal of Materials Science **44**, 3241 (2009).

[35] C J. Hoogerbrugge and J. M. V. A Koelman, Europhysics Letters, **19**, 155 (1992).

[36] P. Español and P. Warren, Europhysics Letters, **30**, 191 (1995)

[37] G. Pan and C. W. Manke, Journal of Rheology, **46**, 1221, (2002)

[38] J.A. Elliott, and A.H. Windle, Journal Chemical Physics, **113**, 10367, (2000).

[39] E. S. Boek, P. V. Coveney, H. N. W. Lekkerkerker, P. van der Schoot, Physical Review E, **55**, 3124 (1997).

[40] N. S. Martys, Journal of Rheology, **49**, 401, (2005).

[41] J.A. Elliott, M. Benedict, M. Dutt, Molecular Simulation **32**, 1113, (2006).

[42] A. M. Donald and A. H. Windle, Liquid Crystalline Polymers, CUP, Cambridge, 1992.

[43] J. A. Goulet, MPhil Thesis, University of Cambridge (2005)

[44] F. Behroozi, M. Orman, R. Reese , W. Stockton, J. Calvert, F. Rachford, and P. Schoen, Journal of Applied Physics, **68**, 3688, (1990).

[45] L. Benidict, L. Louie and M. Cohen, Physical Review B, **52**, 8541(1995).

[46] B. H. Fishbine, Fullerene Science and Technology, **41**, 87 (1996).

[47] S. Yamamoto, T. Matsuoka, Journal of Chemical Physics, **98** (1), 644 (1993).

[48] K. A. Rose, J. A. Meier, G. M. Dougherty, and J. G. Santiago, Physical Review E **75**, 011503 (2007) and personal communications with K A Rose.

a)

b)

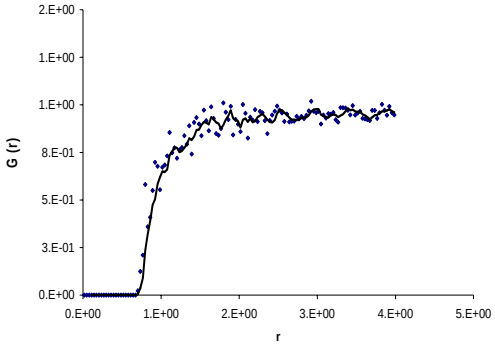

(c)

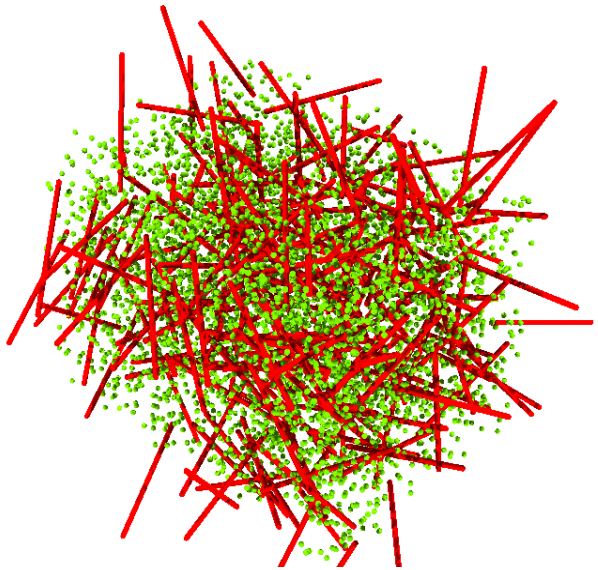

d)

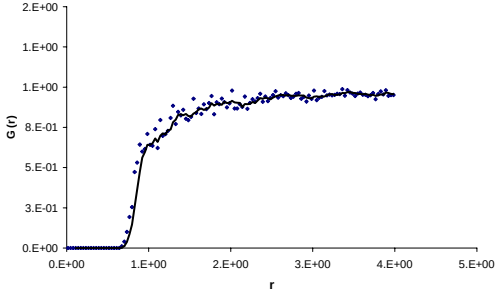

Figure 1. *a) The mixture of fibres (λ = 20) and spheres with total volume fraction Φ_{total} = 0.085 and relative fraction of spheres Φ_{rs} = 0.1*

b) sphere-sphere RDF for the same mixture

c) The mixture of fibres (λ = 20) and spheres with total volume fraction Φ_{total} = 0.095 and relative fraction of spheres Φ_{rs} = 0.5

d) sphere-sphere RDF for the same mixture

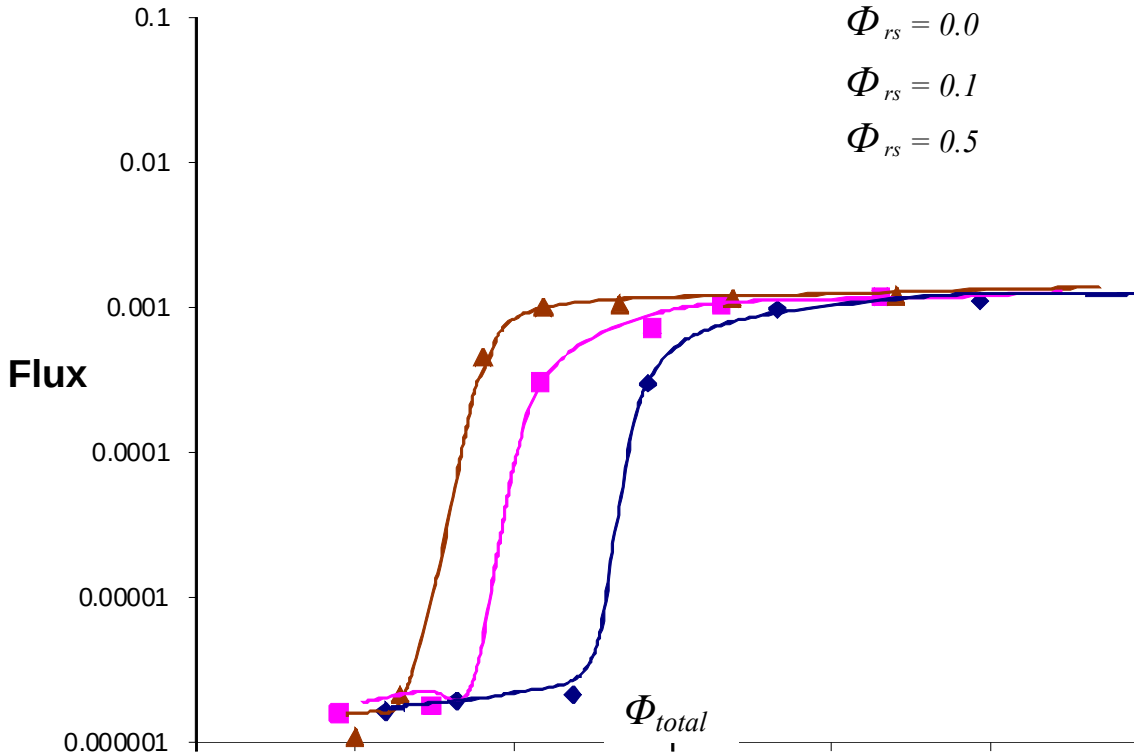

Figure 2. *Percolation transition for fibre spheres mixture for different relative volume fraction of spheres after carrying out* 2×10^6 *Monte Carlo steps.*

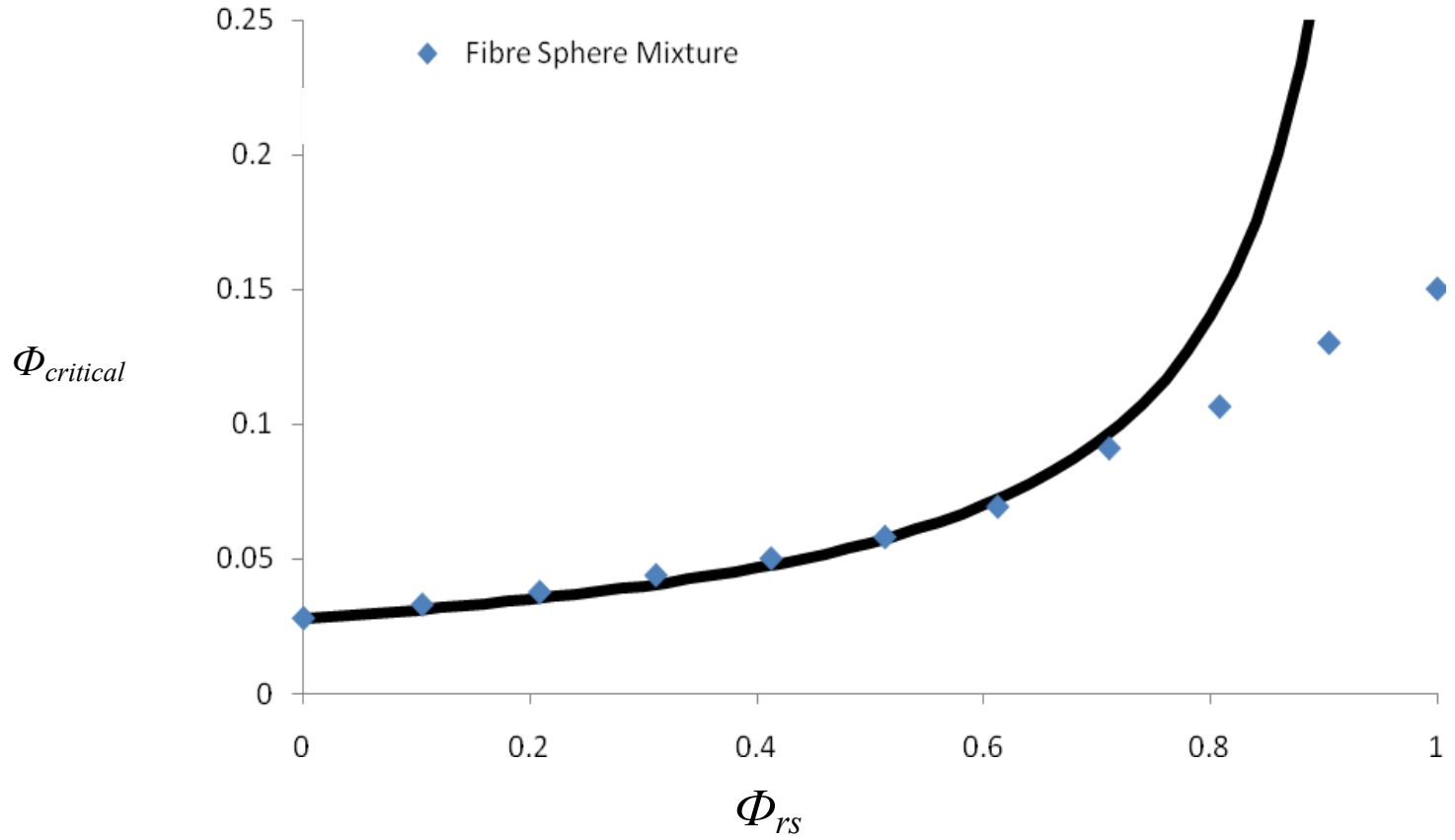

Figure 3. *Critical volume fraction required to achieve percolation as a function of the relative volume fraction of spheres (Φ_{rs}) in the fibre-sphere mixture (The black curve represents the threshold required to achieve percolation in the binary mixture if the spheres do not contribute in formation of percolating network).*

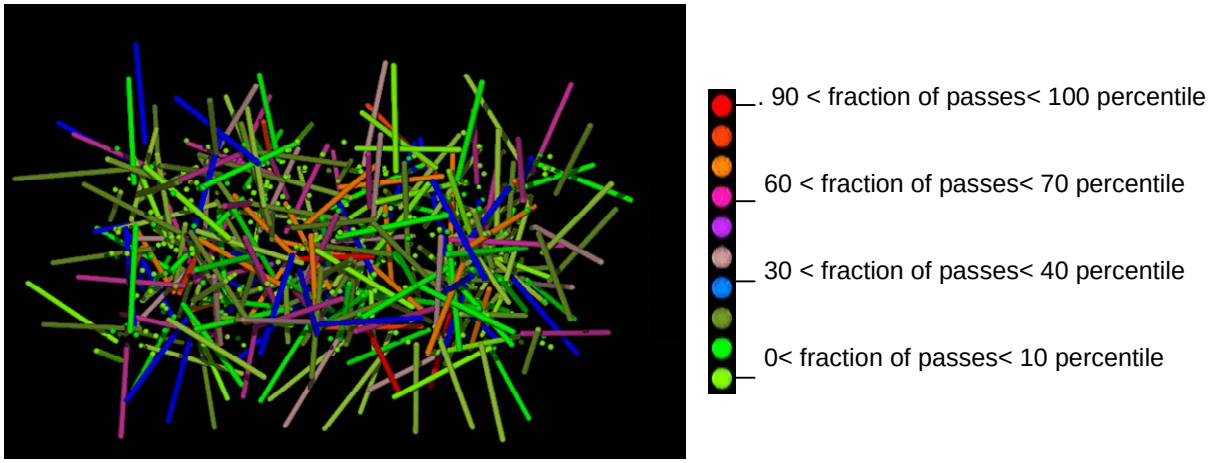

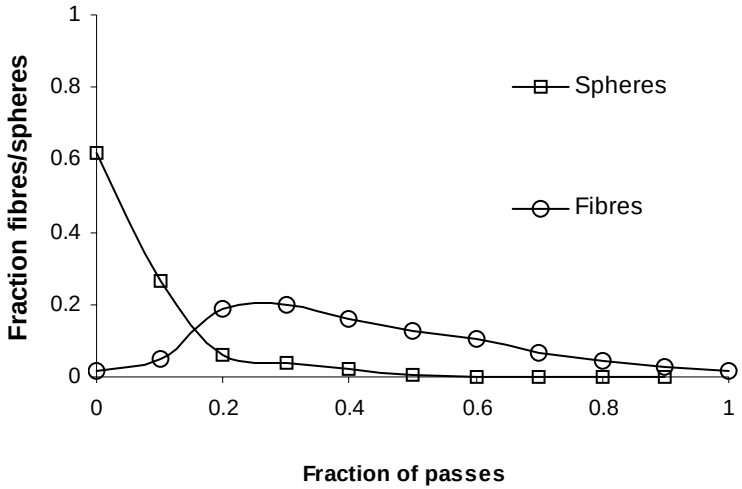

(a) **(b)**

Figure 4a. Binary mixture of fibres(aspect ratio 20) and spheres, with $\Phi_{total} = 0.045$; $\Phi_{rs} = 0.05$. The fibres/spheres are colour-coded according to the frequency of visits during multiple Monte Carlo walks. In the colour scale, red represents most frequently visited sites (between 90 to 100% visits) while green represents least frequently visited sites (less than 10% visited sites).

Figure 4b. Histogram of fibres/spheres visited during the multiple Monte Carlo walk, $\Phi_{total} = 0.045$; $\Phi_{rs} = 0.05$.

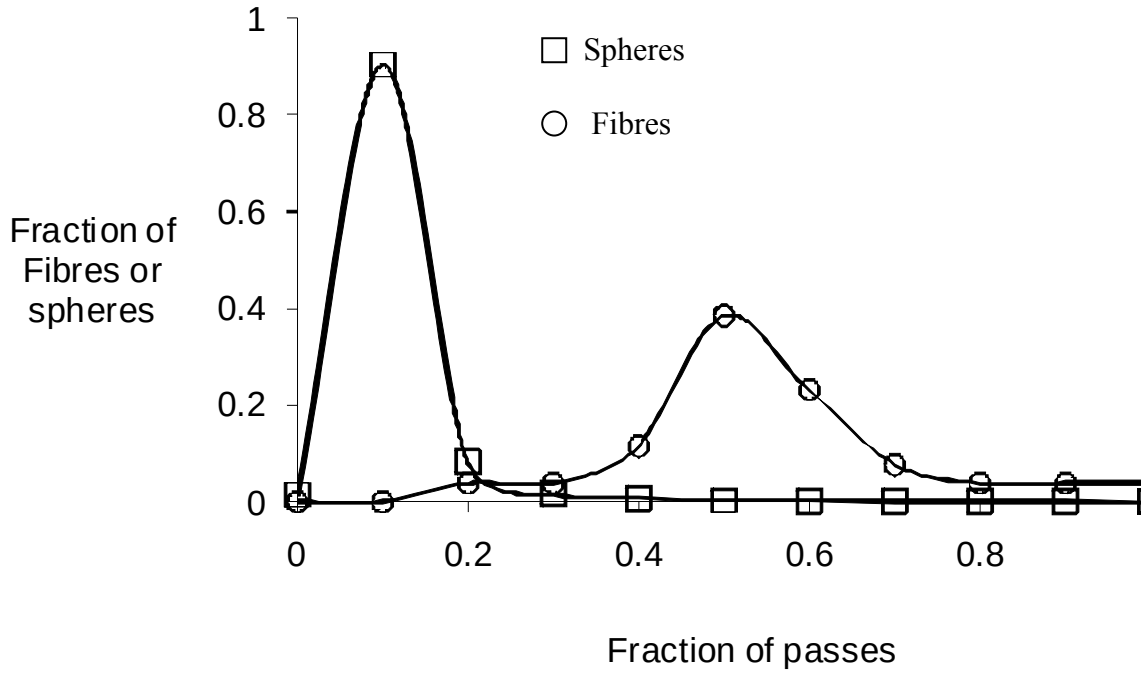

Figure 5. Histogram of fibres and spheres visited during multiple Monte Carlo walks. $\Phi_{total} = 0.14$; $\Phi_{rs} = 0.9$

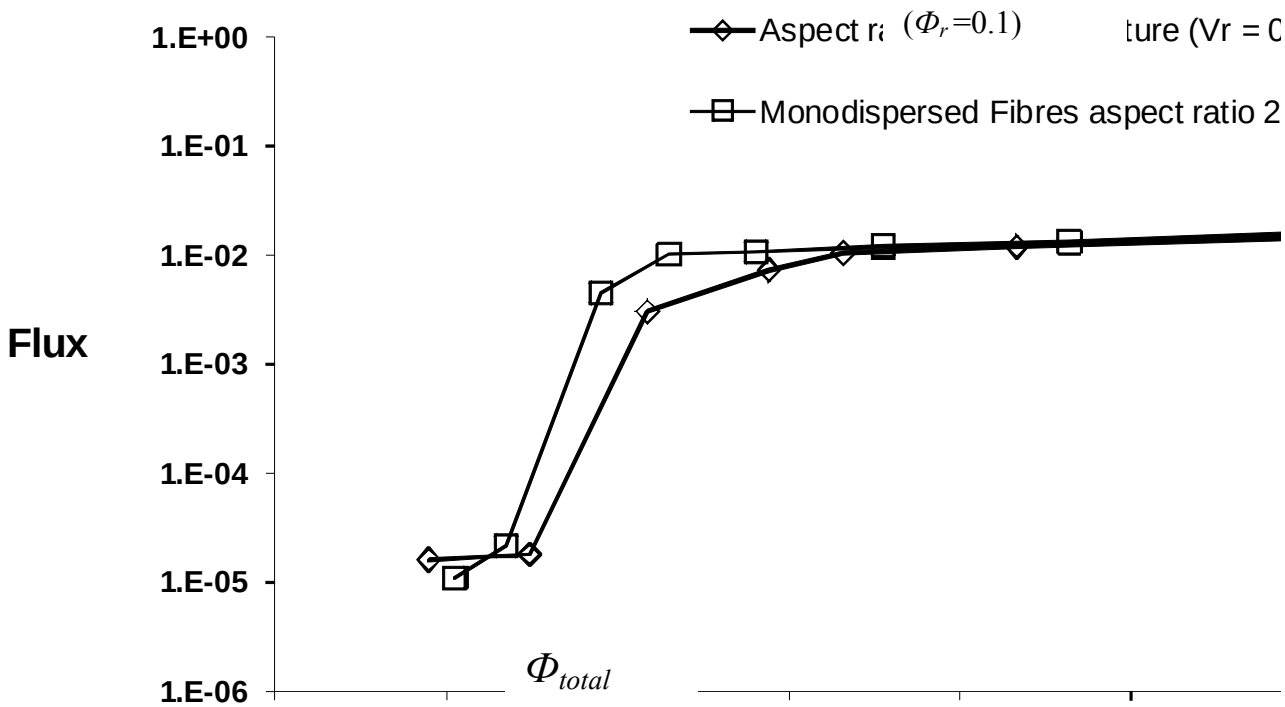

Figure 6. Percolation transition for randomly oriented mono-dispersed fibres of aspect ratio 20 (Φ_r = 0.0, mono-disperse fibres) and a binary mixture of fibres with aspect ratios 5 and 20 ($\Phi_r(\lambda=5)$ = 0.1, binary mixture).

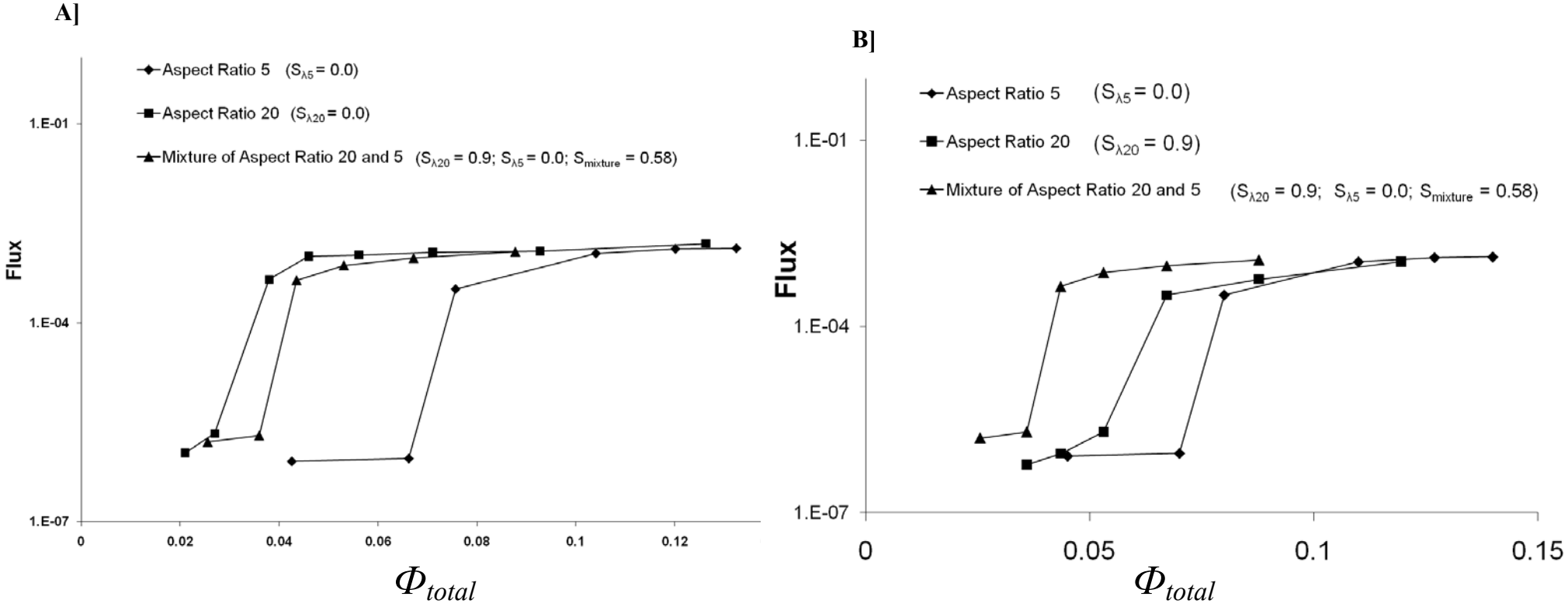

Figure 7a Comparison of percolation transition in mono-dispersed randomly oriented aspect ratio 20 fibres ($s_{\lambda20}$ = 0.0) and mixture of fibres of aspect ratio 20 ($s_{\lambda20}$ =0.9) and aspect ratio 5, ($s_{\lambda5}$ = 0 and $s_{mixture}$ = 0.58).

Figure 7b Comparison of percolation transition of aligned mono-dispersed fibres of aspect ratio 20 ($s_{\lambda20}$ =0.9) with mixture of fibres of aspect ratio 20 ($\langle S_{\lambda20} \rangle$ = 0.9) and aspect ratio 5 ($s_{\lambda5}$ =0 and s_{mixture} = 0.58) and with aligned fibres (λ = 20 $s_{\lambda20}$ = 0.0). The mixture of fibres ensemble shows percolation transition at lower volume fraction than monodispersed aligned fibres of aspect ratio 20 ($s_{\lambda20}$ = 0.9).

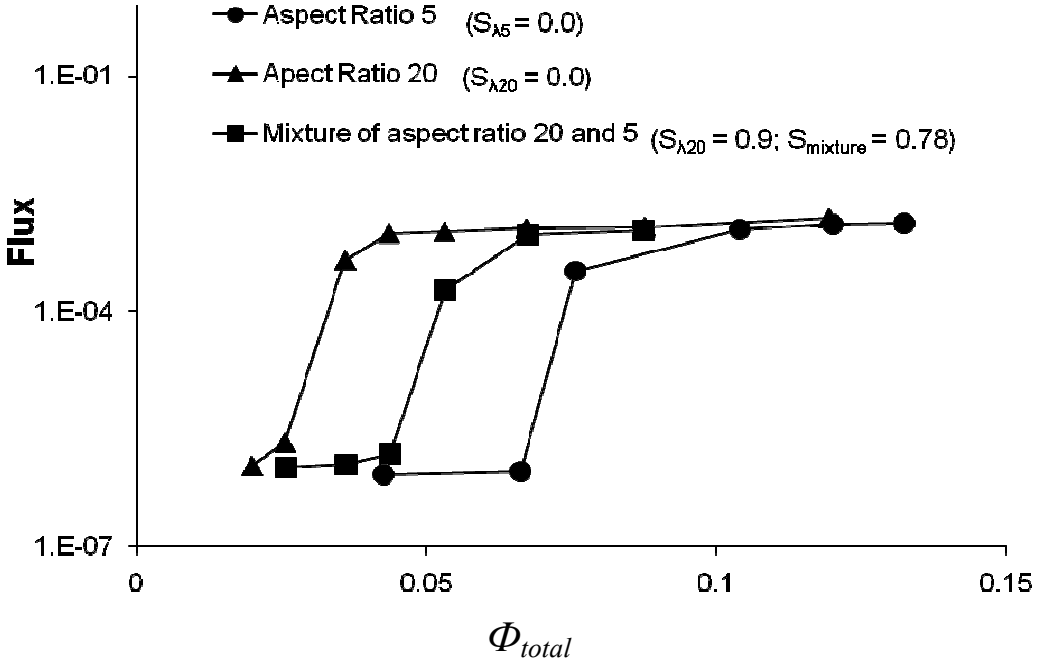

Figure 8a Comparison of percolation transition in monodispersed randomly oriented aspect ratio 20 fibres ($s_{\lambda 20}$ = 0.9), aspect ratio 5 fibres ($s_{\lambda 5}$ = 0.9) with the partially aligne ixture of aspect ratio 20 and aspect ratio 5 fibres.

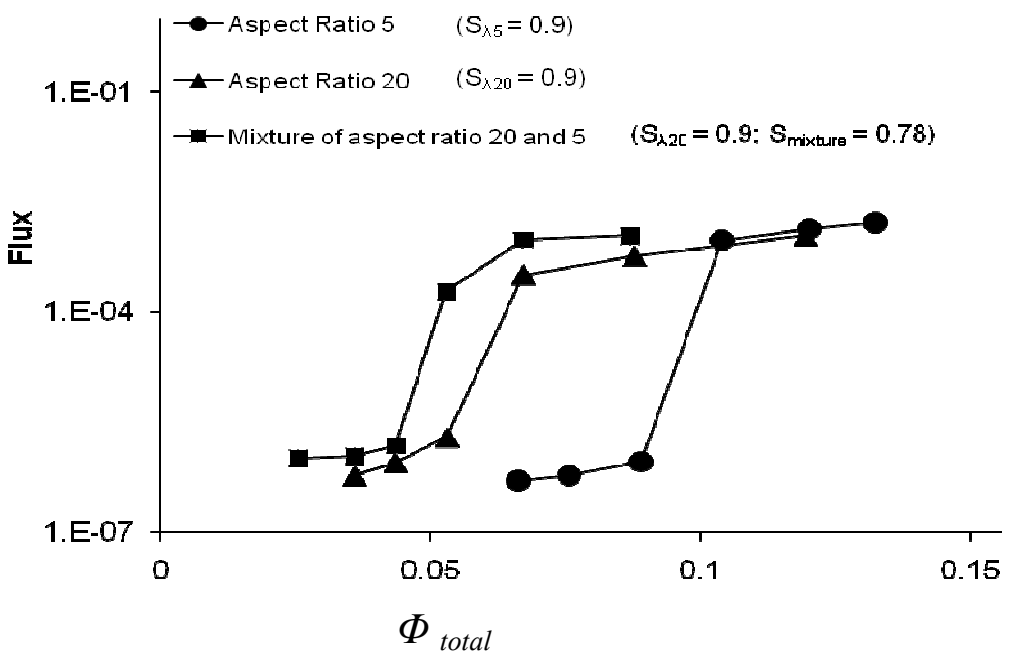

Figure 8b Comparison of percolation transition in monodispersed partially aligned aspect ratio 20 fibres ($s_{\lambda 20}$ = 0.9), aspect ratio 5 fibres ($s_{\lambda 5}$ = 0.9) with the partially aligned mixture of aspect ratio 20 and aspect ratio 5 fibres.